Korean J. Chem. Eng., 37(6), 1050-1056 (2020)
DOI: 10.1007/s11814-020-0528-z

pISSN: 0256-1115
eISSN: 1975-7220

Intrinsically microporous oligomers as organic porogens for mixed-matrix membranes

Gi Hyeon Moon, Sungjin Park, Seul Chan Park, Byung Su Kim, Jaeyoung Jang, and Yong Soo Kang†

Department of Energy Engineering, Hanyang University, Seoul 04763, Korea
(*Received 12 December 2019 • accepted 28 February 2020*)

Abstract−Intrinsically microporous oligomers (or oligomers of intrinsic microporosity, OIM) for use as organic porogens were first synthesized and subsequently incorporated into polysulfone (PSU) matrices to produce mixed-matrix membranes (MMMs) for gas separation. Their molecular weight was controlled to be about M_n=2,800 (n~5-6), and their end groups were regulated to be either -OH (OH-OIM) or -F (F-OIM) for improvement in the compatibility between OIM and PSU. The intrinsic pores of OIM greatly increase the gas permeability of PSU with only a small loss of gas selectivity. For instance, 20/80 wt% OH-OIM/PSU MMMs yield up to three- to four-fold higher permeability of CO_2 and He compared to neat PSU, mostly associated with the intrinsic pores of OIM and its high compatibility with PSU. Additionally, very little reduction in separation performance was observed over 100 days. This suggests OIM as a promising organic porogen of MMMs for improving gas separation performance.

Keywords: Gas Separation, Mixed-matrix Membranes, Organic Porogen, Permeability, Selectivity

INTRODUCTION

Membrane processes utilizing polymeric materials for gas separation are widely used because of their advantages in cost and processability compared to other separation processes such as distillation and pressure-swing adsorption [1]. Despite the advantages of polymeric materials, they have a limitation in improving gas separation performance, described commonly as the "upper bound" [2]. A large body of research has been conducted to overcome the upper bound. One such approach is to incorporate porous or nonporous materials such as silica, zeolites, metal-organic frameworks (MOFs), carbon molecular sieves (CMSs), carbon nanotubes, and graphenes into a polymer matrix to produce mixed matrix membranes (MMMs).

Conventionally, MMMs are made with organic and inorganic complexes to obtain the advantages of both. Typical MMMs consist of a bulk organic polymer called "matrix" and inorganic particles called "fillers" that can be either porous or nonporous [3].

Permeation properties through MMMs with non-porous fillers have been commonly expressed by the Maxwell model [4,5] without considering the interfacial properties, resulting in the decrease in the permeability with the amount of the filler primarily due to the tortuous diffusion path. However, there have been some cases of MMMs whose gas separation performance deviated from the Maxwell model [6]. For example, higher permeability with improved selectivity for condensable gases such as CH_4 was achieved by incorporating non-porous nanosilica fillers into a polymeric matrix for separation of CH_4/H_2 [6]. These results suggest that the interfacial structure and properties associated with incompatibility between the matrix and filler surface could be critically important in determining separation performance. Several studies have utilized interfacial properties to enhance gas permeability with non-porous fillers [7,8].

Additional enhancement of overall gas separation can be obtained by employing porous fillers or porogens, which have proper pore sizes for specific gas pairs, and additionally by generating micropores at the interface between the polymeric matrix and porous filler surface [4,5]. The size and amount of interfacial micropores are primarily dictated by compatibility, but fine tuning of the size and amount of interfacial micropores is not easy. Nonetheless, many improvements in separation performance have been achieved, and their results have been rigorously reviewed [9-11]. Several attempts to improve the compatibility between matrix and filler have been made by introducing an organophilic filler surface. Organic and organic-inorganic hybrid fillers have been introduced because they are more intrinsically compatible with organic matrices [12,13].

Organic-inorganic hybrid fillers such as MOFs have improved compatibility and interfacial properties compared to inorganic fillers such as zeolite and silica [14]. MOFs have a wide scope of applications because they are tunable with regard to chemical groups, pore volume and shape, and surface area, which affect gas transport properties [15]. Such tunability significantly improves the separation performance of MMMs to reach target values. Although MOFs have several advantages, scale-up of production and hydrothermal stability are major obstacles for industrial applications [16]. Consequently, organic fillers such as covalent organic frameworks (COFs) [17], porous organic frameworks (POFs) [18], and porous organic cages (POCs) [19-21] have been investigated for the additional chemical and hydrothermal stability associated with their irreversible covalent bonding.

Porous organic fillers have also shown excellent gas permeation properties while maintaining their selectivity change minimum. POF/PIM-1 MMMs showed CO_2 permeability two-fold higher than that of neat PIM-1 alone while maintaining CO_2/N_2 selectivity nearly unchanged, where POFs were created by reacting melamine with

†To whom correspondence should be addressed.
E-mail: kangys@hanyang.ac.kr
Copyright by The Korean Institute of Chemical Engineers.

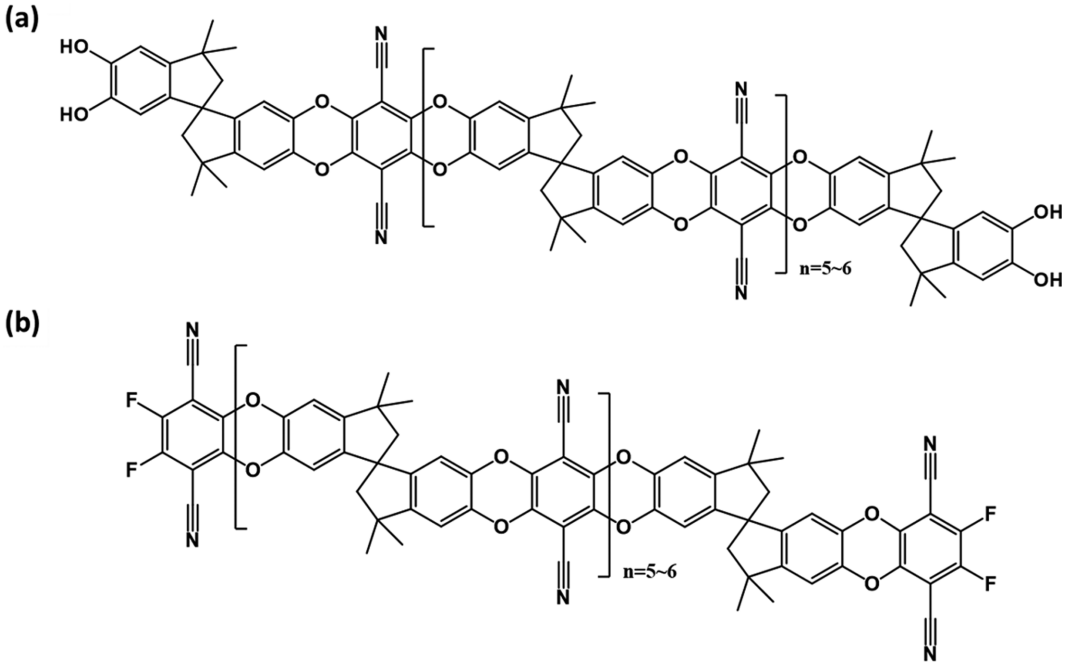


Fig. 1. Chemical structures of (a) OH-OIM with OH end groups and (b) F-OIM with F end groups.

1,4-piperazinedicarboxaldehyde [22]. An MMM of microporous zinc-linked COF (ACOF-1) combined with a commercial polymer (Matrimid 5218) resulted in improved separation performance for a CO_2/CH_4 equimolar mixture [23]. SEM and Raman spectroscopy were utilized to confirm uniform dissolution of the filler. Vertex-functionalized amorphous scrambled porous organic cages (ASPOCs) were also utilized as organic filler into the Matrimid matrix [24]. The CO_2 permeability was fourfold higher and the N_2/SF_6 selectivity threefold higher than that of neat Matrimid. EDX and Raman mapping techniques were used to confirm the uniform distribution of ASPOCs in the polymer matrix.

Highly porous organic polymers such as polymers with intrinsic microporosity (PIMs) and poly[1-(trimethylsilyl)-1-propyne] (PTMSP) [25] have been frequently used as organic fillers to enhance gas separation because of their extremely high gas permeability. Chemical structure of PIM-1, the first PIM developed, having intrinsic micropores as defined by IUPAC (pore size <2 nm), is in Fig. 1, but the degree of polymerization n is typically around 200-300. For instance, PIM-1 was incorporated into either a polyetherimide matrix (Ultem) [26] or polyimide matrix (Matrimid) [27] to produce an MMM. The permeability of PIM-1/Ultem 20/80 wt% MMMs was two-fold higher than that for overall gas species. No interfacial defects between filler and matrix were observed in this experimental range. However, above 20 wt% PIM-1, a phase-separated structure was observed due to the high molecular weight of PIM-1 [28]. In this regard, the compatibility between a host polymer matrix and filler should be increased to improve the separation performance further, even though organic fillers are more compatible than inorganic ones.

We anticipate that organic porogens with low molecular weight will improve compatibility with a common matrix polymer and increase the loading amount for uniformly dissolved MMMs. We propose oligomers for intrinsic microporosity (OIM, its chemical structure is drawn in Fig. 1) as a new organic porogen to improve gas separation performance.

In this study, we focused on the enhanced compatibility derived from both the lower molecular weight and the chain end chemical structure of porous OIMs and its effects on gas separation properties. Improved gas separation performance is explained in terms of the compatibility and the free volume. It was found that polysulfone (PSU) was compatible with OIM up to 40 wt% without any observable phase separation. Therefore, OIM could be widely used as an organic porogen for MMMs because of its porosity and excellent compatibility with polymer matrix.

EXPERIMENTAL

1. Materials

5,5′,6,6′,-Tetrahydroxy-3,3,3′,3′,-tetramethyl-1,1′-spriobisindane (TTSBI, >96.0% (HPLC)) was purchased from Tokyo Chemical Industry (TCI) and purified by recrystallization in methanol. 2,3,5,6-Tetrafluoroterephtahlonitrile (TFTPN, 98%) was purchased from Matrix Scientific and purified using vacuum sublimation. Potassium carbonate (anhydrous, ACS reagent, >99%), N,N,-dimethylformamide (anhydrous, 99.8%), and polysulfone (M_w~35,000 by LS, M_n~16,000 by MO, pellets) were purchased from Sigma Aldrich and used as-received without further treatment. Chloroform (Extra pure, 99.5%) and tetrahydrofuran (THF) (Extra pure, 99%) were purchased from Daejung Chemicals & Metals and used as-received.

2. Synthesis of PIM and OIM

2-1. Synthesis of PIM-1

For this synthesis, 5.437 g TTSBI, 3.195 g TFTPN, and 4.41 g K_2CO_3 were dissolved into 100 ml DMF in a round-bottom flask and stirred for 20 min. The dissolved solution was purged with argon

for 20 min to produce inert conditions. Polymerization of PIM-1 progressed at 70 °C for 72 hours with vigorous stirring (>800 rpm). After 72 hours, 200 ml of THF was added into the flask and stirred for 30 min. The solution then was separated into a precipitated polymer phase and a supernatant solution containing low-molecular weight polymers and cyclic chains. After eliminating the supernatant solution, the precipitated polymers were redissolved into THF and separated into a precipitate containing cross-linked PIM and K_2CO_3 and a supernatant containing high-molecular weight PIM-1. The supernatant was poured into methanol to eliminate residual monomers and redissolved into THF. The redissolved solution was poured into DI water to remove residual K_2CO_3. Finally, a bright yellow PIM-1 powder was collected using vacuum filtration and dried under vacuum at 100 °C for 24 h.

2-2. Synthesis of OH-OIM and F-OIM

This synthesis involved dissolution of 5.437 g TTSBI, 1.6 g TFTPN, 4.41 g K_2CO_3 for F-OIM and 5.437 g TTSBI, 4.26 g TFTPN, and 4.41 g K_2CO_3 for OH-OIM into 100 ml DMF in a round-bottom flask and stirring for 20 min. The dissolved solution was purged with argon for 20 min to create inert conditions. OIM was formed at 60 °C for 48 hours with vigorous stirring. The solution was poured into DI water to eliminate residual K_2CO_3 and redissolved into THF. The redissolved solution was poured into methanol to eliminate the residual monomers. This elimination process was repeated three times. Crude dark-brown oligomer OIM powder was obtained using vacuum filtration and dried under vacuum at 100 °C for 24 h.

3. Free-standing MMM Film Preparation

For MMM films, 2 wt% concentrations of polysulfone (PSU) and OIM were dissolved in chloroform and stirred for 48 or 24 hours, respectively. The PSU/OIM blend solution was produced by mixing PSU and OIM solutions at varying weight content. After 48 hours of stirring, the blend solution was degassed for 30 min, filtered through a 0.45 μm PVDF syringe filter, and cast onto a flat-bottom glass dish placed in ambient conditions for three days. The cast film was dried under vacuum at 100 °C for 48 h to eliminate residual solvents.

4. Characterizations

Chemical structures of PIM-1, OIM, and end groups were characterized using ^{1}H nuclear magnetic resonance (^{1}H NMR) spectroscopy with a VNMRS 600 MHz instrument (Agilent technologies) and Fourier-transformed infrared spectroscopy (FT-IR) with an FT-IR 4200 instrument (Jasco) with an attenuated total reflectance (ATR) accessory. Molecular weights of PIM-1 and OIM were measured using gel permeation chromatography (GPC) with an Ultimate 3000 instrument (Thermo Fisher Scientific). KF-806L column with THF solvent was used for GPC measurements. Also, matrix assisted laser desorption ionization time-of-flight (MALDI-ToF) mass spectrometry with AXIMA instrument (SHIMADZU-biotech) was utilized for molecular weight measurements. BET (Brunauer-Emmett-Teller) surface area measurement was conducted with surface area & pore size analyzer with 3Flex (Micromeritics). 12 mm long tube was used for sample preparation. Nitrogen gas was used as adsorption gas at 77 K. Phase separation or dispersity of PIM-1 and OIM in the PSU matrix was confirmed using atomic force microscopy (AFM) with an XE-100 instrument (Psia) installed at Hanyang LINC+ Analytical Equipment Center (Seoul). The arithmetic mean value R_a and the root mean square value R_q were calculated with the XEI (Park System) program. Also, microstructures of MMMs were measured by field emission scanning electron microscope (FE-SEM) with an NOVA nano SEM 450 (FEI) installed at Hanyang LINC+ Analytical Equipment Center (Seoul). Glass transition temperatures of MMMs were measured using differential scanning calorimetry (DSC) analysis with a Q 20 instrument (TA Instruments) and universal analysis 2000. Both of cooling and heating rate were 20 k/min. For resetting thermal history of MMMs, the samples were first heated to 300 °C and cooled to room temperature. The data of DSC thermograms were given at 2nd heating process. Densities of MMMs were measured using a balance (MSE224S-000-DU, Sartorius) with a density kit relying on Archimedes' principle, which can be expressed by Eq. (1):

$$\rho_{film} = \frac{w_a}{w_a - w_l} \times \rho_l \quad (1)$$

where ρ_{film} is the film density, w_a and w_l are the film weight in air and liquid, respectively, and ρ_l is the density of liquid. 2,2,4-Trimethylpentane was used for the auxiliary liquid.

Fractional free volume (FFV) of MMMs was calculated using Eq. (2):

$$FFV = \frac{V - V_o}{V} \quad (2)$$

Specific volume of polymer V is calculated using the measured density. Occupied volume of polymer V_o is calculated using the equation $V_o = 1.3V_w$, where V_w is the van der Waals volume estimated by the group contribution [29]. For MMMs, V_w is calculated using Eq. (3):

$$V_w = w_m V_{wm} + w_f V_{wf} \quad (3)$$

where w_m and w_f are molar fractions of matrix and filler, respectively, and V_{wm} and V_{wf} are the van der Waals volumes.

Gas transport properties were measured using constant-volume/variable-pressure permeation cells. Applied pressure was 1 atm, and film thickness was 50 μm. Pure gas permeability was calculated from the slope between time and pressure change in a downstream constant-volume chamber, and the ideal separation factor (α_{12}) was obtained using the relationship $\alpha_{12} = P_1/P_2$, where P_i is the permeability of pure gas *i*.

RESULTS AND DISCUSSION

1. Preparation and Characterization of OIM

The molecular weight and end groups of oligomers and polymers are readily controlled by adjusting the molar ratio of two monomers as described by the Carothers equation for polycondensation process [30]. In this study, we utilized monomers of TTSBI (5,5′,6,6′,-tetrahydroxy-3,3,3′,3′,-tetramethyl-1,1′-spriobisindane) and TFTPN (2,3,5,6-tetrafluoroterephtahlonitrile) to prepare oligomers with intrinsic microporosity (OIMs) with different end groups. Depending on monomer ratio, OIMs with OH groups (OH-OIMs) and OIMs with F groups (F-OIMs) at the chain ends were readily obtained to have the average molecular weight: OH-OIM (M_n=2,632, M_w=3,431) and F-OIM (M_n=2,914, M_w=3,537) which were measured by

GPC. Thus, the chemical structure of the repeating unit for OIMs is identical to that of PIM-1, but with different molecular weight and controlled end groups, as shown in Fig. 1 The end groups of F-OIM were first characterized by a peak at −135 ppm for ^{19}F NMR spectroscopy (Fig. S1); OH-OIM did not have a similar peak (Fig. S2). FT-IR spectra (Fig. S3) confirm the existence of the hydroxy group (3,100-3,700 cm^{-1}) on OH-OIM and its absence on F-OIM.

For identification of linear chain formation, molecular weights of OH-OIM and F-OIM were measured again with MALDI-ToF (Fig. S4). The molecular weights of both OIMs were detected in the expected ranges following the GPC results and their intervals were also confirmed to be similar with the repeating unit of PIM-1 (500 Da). Between every interval, there were no obvious peaks, presenting the formation of mostly linear chains [31].

The three-dimensional (3D) structures of OH-OIM and F-OIM are shown in Fig. 2 The chain lengths of both OH-OIM and F-OIM are sufficiently long to form intrinsic micropores, primarily resulting from the spirocenter of the molecular structure. Therefore, they can be utilized as organic porogens with micropores.

To verify the micropores in OIMs more precisely, BET (Brunauer-Emmett-Teller) surface area measurements were conducted. The specific surface area of OH-OIM and F-OIM is 105.93 and 81.77 m^2/g, respectively. The surface area of OIM is enormously higher than common polymers like polyethylene (0.13 m^2/g) [32], polyacrylonitrile (7.03 m^2/g) [33] and also polysulfone (<1 m^2/g) [34]. Although it is lower than that of PIM-1 (793.19 m^2/g), it is reasonable to argue that OIM are microporous, which is consistent with the fact that the fractional free volume of PIM-1 is reduced when the molecular weight is decreased [35]. This is because PIM-1 chains with low molecular weights are more easily packed with each other than those with high molecular weight.

2. Compatibility and Chain Mobility

To confirm the compatibility between OIM and PSU matrix, the relation between glass transition temperature (T_g) and weight fraction of porogens (w_1) was utilized. If polymer blends are compatible with each other to form a homogeneous phase, the inverse of glass transition temperature ($1/T_g$) of the blend and the weight fraction of the porogen (w_1) have a linear relation according to the

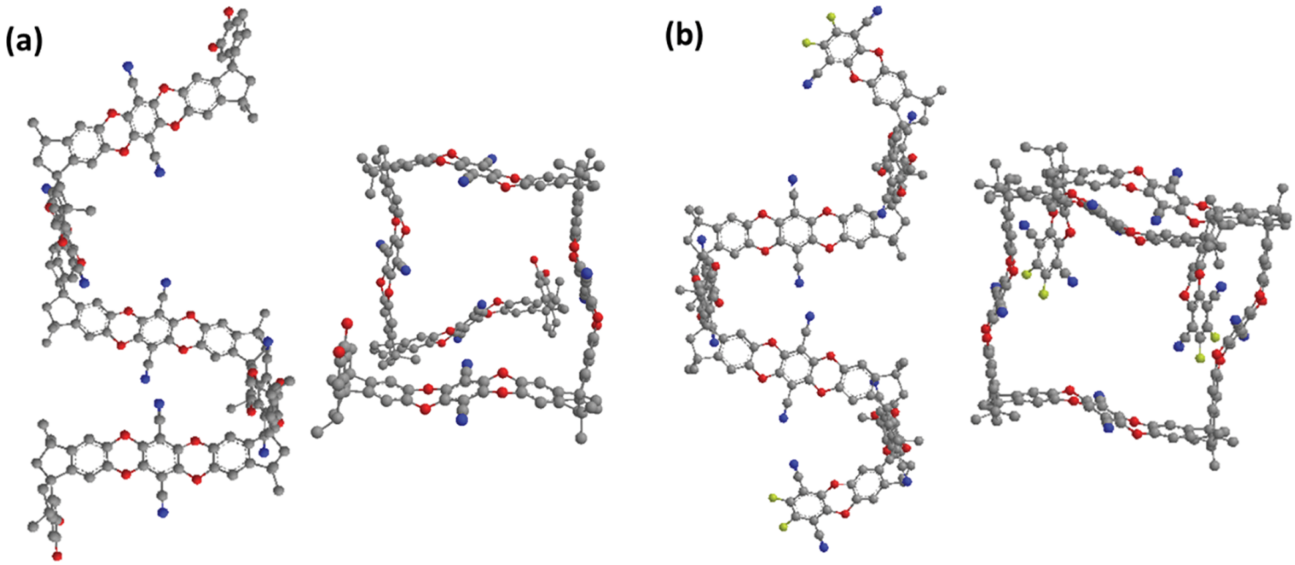


Fig. 2. 3D molecular models of (a) OH-OIM and (b) F-OIM from various viewpoints.

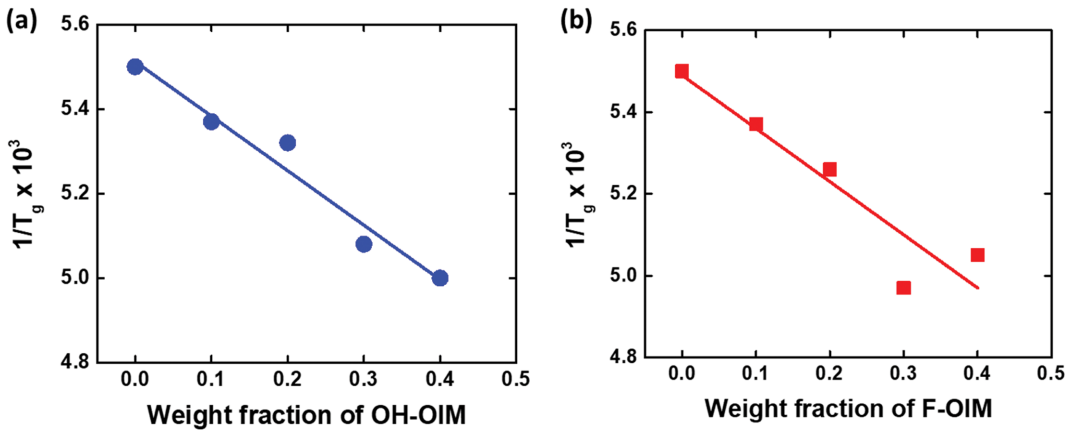


Fig. 3. The inverse of glass transition temperature of OIM/MMMs with various weight fraction of (a) OH-OIM and (b) F-OIM.

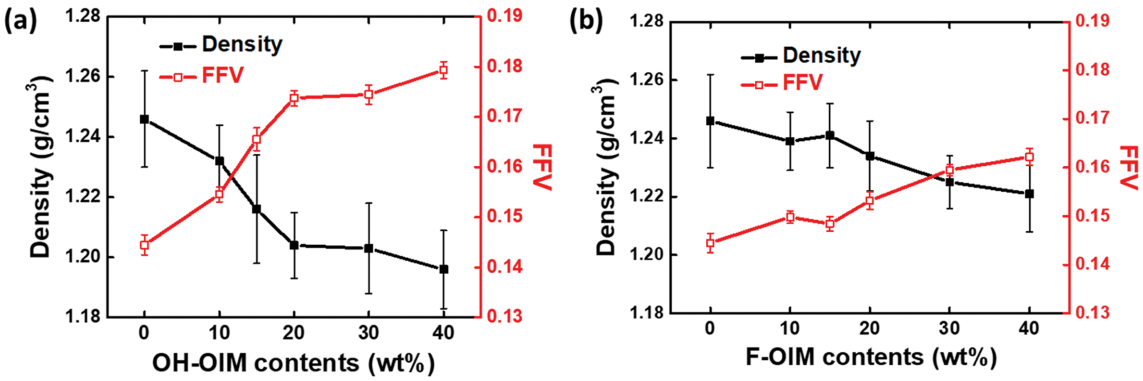


Fig. 4. The density and fractional free volume of (a) OH-OIM/PSU and (b) F-OIM/PSU as a function of porogen weight fraction.

Fox model (Eq. (4)) [36]. Fig. 3 illustrates a linear relation between $1/T_g$ and w_1, suggesting the miscibility up to 40 wt% for OH-OIM with PSU.

$$\frac{1}{T_g}=\frac{w_1}{T_{g,1}}+\frac{w_2}{T_{g,2}}=\left(\frac{1}{T_{g,1}}-\frac{1}{T_{g,2}}\right)w_1+\frac{1}{T_{g,2}} \quad (4)$$

where $T_{g,1}$ and $T_{g,2}$ are the glass transition temperature of OIM and PSU, respectively, with w_2 being the weight fraction of PSU ($w_1+w_2=1$).

The compatibility was further verified by cross-sectional SEM (Fig. S5) and surface AFM (Fig. S6) images. Both SEM and AFM images show that the 20 wt% PIM-1/PSU image exhibits significant phase separation because of their incompatibility. On the other hand, OH-OIM/PSU and F-OIM/PSU showed rather homogeneous images within 10-30 wt% of OIM content, which are very similar to neat PSU. The SEM and AFM images are consistent with the change in T_g with the amount of OIMs (Fig. 3). These suggest that the lower molecular weight OIM is much more compatible with PSU than the high molecular weight PIM-1 because of larger entropic contribution of OIM on the Gibbs free energy of mixing (details in supplementary information p.7).

Glass transition temperature (T_g) is a measure of chain mobility at fixed molecular weight. Fig. 3 shows how T_g of MMMs increases from 181 °C to 201 °C as the porogen content increases to 40 wt%. The increase in T_g can be explained by the restricted PSU chain mobility by OIM because of its super-glassy characteristics. No significant difference in T_g between OH-OIM and F-OIM MMMs indicates that the chain mobility decreases with the amount of OIM regardless of the end group because of the super-glassy OIM structure; the end group effects of OH- and F-groups on T_g are not significant.

3. Fractional Free Volume

As OIM porogens were added, the densities of OIM/PSU MMMs decreased, and the fractional free volume (FFV) expanded (Fig. 4) because OIM has micro-sized pores, as shown in Fig. 2. FFV was estimated using Eq. (2), with $FFV=(V-V_o)/V$, where V is the specific volume measured from the density, and V_o is the occupied volume of polymer estimated by $V_o=1.3V_w$, with V_w being the van der Waals volume obtained using the group contribution method [32]. The intrinsic microporosity in the OIM porogen contributes to introduction of additional micropores in OIM/PSU MMMs. OH-OIM may generate the larger amount of free volume in MMMs than F-OIM at the same porogen content. This may be because OH-OIM has more spirocenters than F-OIM, because the spirocenter presumably hinders the chain packing structurally, as shown in Fig. 1, resulting in the higher fractional free volume of OH-OIM. BET surface area of OIMs also supports the higher free volume of OH-OIM from its chain structure.

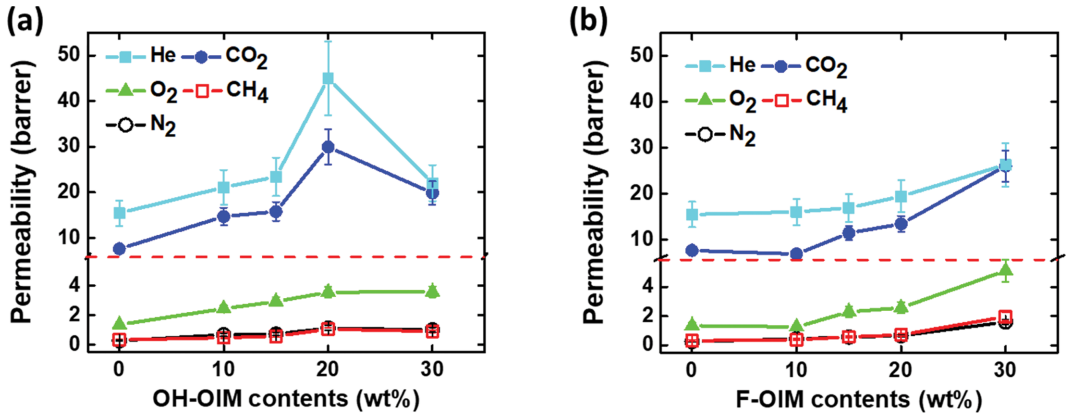


Fig. 5. Pure gas permeability of He, CO_2, O_2, CH_4, and N_2 through (a) OH-OIM/PSU and (b) F-OIM/PSU MMMs at various weight ratios of OIM porogens.

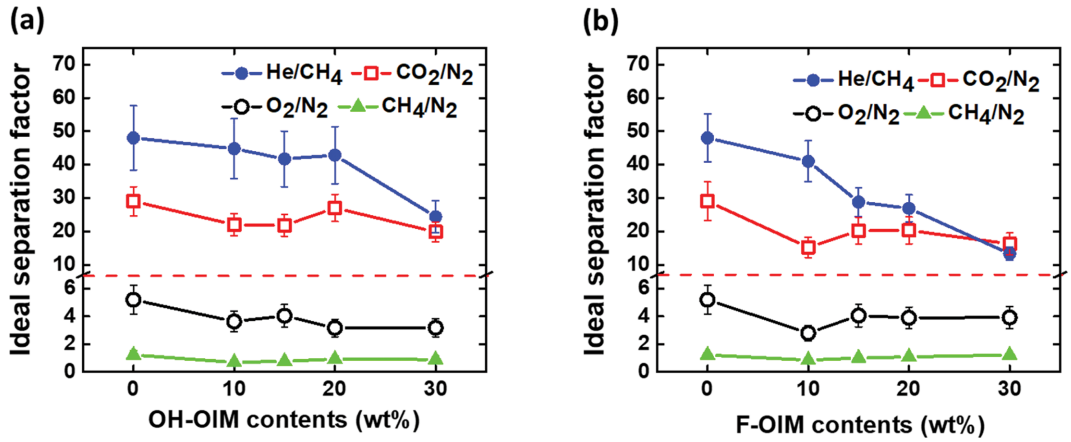


Fig. 6. Ideal separation factor for He/CH_4, CO_2/N_2, O_2/N_2, and CH_4/N_2 gas pairs through (a) OH-OIM/PSU and (b) F-OIM/PSU MMMs at various weight ratios of OIM porogens.

4. Gas Permeation Properties

Pure gas permeabilities and ideal separation factors for He, CO_2, O_2, N_2, and CH_4 through MMMs are illustrated in Fig. 5 and Fig. 6, respectively. For OH-OIM/PSU MMMs, the pure gas permeability of He or CO_2 sharply increases as the concentration of OH-OIM increases, reaching a maximum at 20 wt% OH-OIM, followed by a decrease in the permeability. The permeability behaviors of O_2, N_2, and CH_4 were nearly identical to those of He and CO_2, but the effect was not significant (Fig. 5(a)). For F-OIM/PSU MMMs, the permeability increases monotonically as the concentration of F-OIM increases (Fig. 5(b)).

This permeability enhancement is primarily due to the increase in the fractional free volume of OIMs, as shown in Fig. 4. However, OIM also restricts chain mobility as evidenced by the increase in T_g with the OIM concentration (Fig. 3), presumably causing the decrease in the permeability as observed in common polymers [37]. In other words, the effects of OIMs on free volume and chain mobility are in conflict in this particular system, resulting a maximum permeability at a concentration of OH-OIMs. Over the 20 wt% OH-OIM content, the gas permeabilities of small-sized He and CO_2 decreased significantly, whereas those of rather large-sized O_2, N_2 and CH_4 decreased insignificantly. At this moment, it would be difficult to explain such results at molecular level. However, it may be anticipated that the free volume effect could be dominant in the range of the OH-OIM concentration up to 20 wt%, whereas the rigidified chain effect could be dominant at the OH-OIM concentrations higher than 20 wt% as shown in Fig. 3 and Fig. 4. In the case of F-OIMs, the increase in the fractional free volume is not as significant as OH-OIMs, whereas the increase in T_g is nearly similar to that for OH-OIMs. The gas permeability does not show a maximum, but continuously increases with the F-OIM concentration.

The ideal separation factor through OIM/PSU MMMs decreases slightly as OIM porogen content increases (Fig. 6). The decrease in the ideal separation factor for He/CH_4 is marginal even when the OH-OIM content is as high as 30 wt%.

Consequently, adding a new OIM porogen to the PSU matrix results in the increase in the gas permeability up to fourfold with little sacrifice in the ideal separation factor. For instance, OH-OIM/PSU (20/80 wt%) MMM showed the increases in the CO_2 and He permeability up to 400% and 300%, respectively, with the small decrease in the CO_2/N_2 and He/CH_4 ideal separation factors only 6% and 10%, respectively.

The improvement in the gas separation performance by incorporating OH-OIM into a PSU matrix was illustrated on Robeson's upper bounds [38]. As can be seen in Fig. S7, the results of the current work do not surpass the upper bounds. One reason could be due to the choice of PSU as a host polymer matrix. However, the current work can provide an efficient, simple pathway to improve the gas permeability with little sacrifice of the selectivity.

OIM is highly porous, consequently expecting the permeability decrease with time for MMMs. Therefore, the permeability change over time for 20 wt% OH-OIM/PSU MMM was measured and plotted in Fig. 7 along with PIM-1. The CO_2 permeability through OH-OIM/PSU 20/80 wt% MMM was nearly unchanged even after 100 days, whereas PIM-1 showed a decrease in the CO_2 permeability to nearly half of its original value after 100 days (Fig. 7).

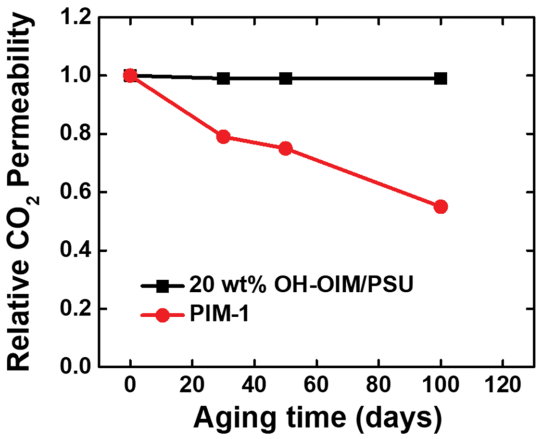


Fig. 7. Relative CO_2 permeability of PIM-1 and 20 wt% OH-OIM/PSU MMM with elapsed time: The initial CO_2 permeabilities for PIM-1 and 20 wt% OH-OIM/PSU MMM were 9692 and 30 barrer, respectively.

CONCLUSIONS

We synthesized a new organic porogen, OIM, with a low molecular weight M_n of 2,600-2,900. The OIM chain ends were chemically controlled to have either OH or F groups (OH-OIM and F-OIM, respectively). OIM was found to be much more compatible with PSU than PIM-1, which has the same chemical structure but a much higher molecular weight. Both F-OIM and OH-OIM dissolved much better than PIM-1 in PSU matrix. These porogens did not show significant phase separation, even at concentrations higher than 30 wt%, demonstrating a much higher compatibility with PSU than PIM-1. The MMM fractional free volume increased as the OIM concentration increased due to the OIM micropores. The increased free volume effect is higher in OH-OIM than in F-OIM because of the higher concentration of the spirocenters in OH-OIM. However, PSU chain mobility was restricted by the superglassy characteristics of OIM. The permeability of OH-OIM/PSU 20/80 wt% MMM was highest, resulting in up to four-times greater permeability with little sacrifice of selectivity. This may be due to the conflicting effects of free volume increase and chain mobility decrease with OH-OIM content. OH-OIM/PSU 20/80 wt% MMMs showed almost no separation performance changes for up to 100 days. Due to its compatibility with common polymeric matrices and high porosity, OIM is a promising porogen for improving gas permeability with little sacrifice of selectivity.

ACKNOWLEDGEMENTS

This work was supported by the Korea Center for Artificial Photosynthesis (KCAP) located in Sogang University and funded by the Ministry of Science, ICT, and Future Planning (MSIP) through the National Research Foundation of Korea (Grant No. 2009-0093883). The surface images (AFM) were analyzed on an XE-100 instrument (Psia) installed at Hanyang LINC+ Analytical Equipment Center (Seoul).

SUPPORTING INFORMATION

Additional information as noted in the text. This information is available via the Internet at http://www.springer.com/chemistry/journal/11814.

REFERENCES

1. M. Galizia, W. S. Chi, Z. P. Smith, T. C. Merkel, R. W. Baker and B. D. Freeman, *Macromolecules*, **50**, 7809 (2017).
2. B. D. Freeman, *Macromolecules*, **32**, 375 (1999).
3. Q. Shen, S. Cong, R. He, Z. Wang, Y. Jin, H. Li, X. Cao, J. Wang, B. V. D. Bruggen and Y. Zhang, *J. Membr. Sci.*, **588**, 117201 (2019).
4. T. T. Moore and W. J. Koros, *J. Mol. Struct.*, **739**, 87 (2005).
5. H. V. Thang and S. Kaliaguine, *Chem. Rev.*, **113**, 4980 (2013).
6. T. C. Merkel, B. D. Freeman, R. J. Spontak, Z. He, I. Pinnau, P. Meakin and A. J. Hill, *Science*, **296**, 519 (2002).
7. J. Ahn, W.-J. Chung, I. Pinnau, J. Song, N. Du, G. P. Robertson and M. D. Guiver, *J. Membr. Sci.*, **346**, 280 (2010).
8. J. Ahn, W.-J. Chung, I. Pinnau and M. D. Guiver, *J. Membr. Sci.*, **314**, 123 (2008).
9. M. G. Suer, N. Bac and L. Yilmaz, *J. Membr. Sci.*, **91**, 77 (1994).
10. K. Zarshenas, A. Raisi and A. Aroujalian, *J. Membr. Sci.*, **510**, 270 (2016).
11. E. M. Mahdi and J.-C. Tan, *J. Membr. Sci.*, **498**, 276 (2016).
12. Y. Liu, G. Liu, C. Zhang, W. Qiu, S. Yi, V. Chernikova, Z. Chen, Y. Belmabkhout, O. Shekhah, M. Eddaoudi and W. Koros, *Adv. Sci.*, **5**, 1800982 (2018).
13. Z. V. Singh, L.-L. Tan, M. G. Cowan, Y.-W. Yang, W. Zhang, D. L. Gin and R. D. Noble, *J. Membr. Sci.*, **539**, 224 (2017).
14. J. D. Evans, D. M. Huang, M. R. Hill, C. J. Sumby, A. W. Thornton and C. J. Doonan, *J. Phys. Chem. C*, **118**, 1523 (2014).
15. H. Furukawa, K. E. Cordova, M. O'Keeffe and O. M. Yaghi, *Science*, **341**, 1230444 (2013).
16. J. B. Decoste, M. S. Denny Jr., G. W. Peterson, J. J. Mahle and S. M. Cohen, *Chem. Sci.*, **7**, 2711 (2016).
17. P. J. Waller, F. Gandara and O. M. Yaghi, *Acc. Chem. Res.*, **48**, 3053 (2015).
18. T. Ben, H. Ren, S. Ma, D. Cao, J. Lan, X. Jing, W. Wang, J. Xu, F. Deng, J. M. Simmons, S. Qiu and G. Zhu, *Angew. Chem. Int. Ed.*, **48**, 9457 (2009).
19. G. Zhang and M. Mastalerz, *Chem. Soc. Rev.*, **43**, 1934 (2014).
20. A. G. Slater and A. I. Cooper, *Science*, **29**, aaa8075 (2015).
21. T. Hasell and A. I. Cooper, *Nat. Rev. Mater.*, **1**, 16053 (2016).
22. B. P. Biswal, H. D. Chaudhari, R. Banerjee and U. K. Kharul, *Chem. Eur. J.*, **22**, 4695 (2016).
23. M. Shan, B. Seoane, E. Rozhko, A. Dikhtiarenko, G. Clet, F. Kapteijn and J. Gascon, *Chem. Eur. J.*, **22**, 14467 (2016).
24. G. Zhu, F. Zhang, M. P. Rivera, X. Hu, G. Zhang, C. W. Jones and R. P. Lively, *Angew. Chem.*, **131**, 2664 (2019).
25. R. R. Tiwari, J. Jin, B. D. Freeman and D. R. Paul, *J. Membr. Sci.*, **537**, 362 (2017).
26. L. Hao, P. Li and T.-S Chung, *J. Membr. Sci.*, **453**, 614 (2014).
27. W. F. Yong, F. Y. Li, Y. C. Xiao, P. Li, K. P. Pramoda, Y. W. Tong and T. S. Chung, *J. Membr. Sci.*, **407-408**, 47 (2012).
28. U. W. Gedde, *Polymer physis*, Chapmann & Hall, London (1995).
29. A. Bondi, *J. Phys. Chem.*, **68**, 441 (1964).
30. W. H. Carothers, *T. Faraday Soc.*, **32**, 39 (1936).
31. J. Song, N. Du, Y. Dai, G. P. Robertson, M. D. Guiver, S. Thomas and I. Pinnau, *Macromolecules*, **41**, 7411 (2008).
32. K. N. Fotopoulou and H. K. Karapanagioti, *Mar. Environ. Res.*, **81**, 70 (2012).
33. V. Babu, S. K. Pasha, G. Gupta, C. B. Majumdar and B. Choudhury, *Fiber Polym.*, **15**, 24 (2014).
34. R. W. Baker, *Membrane technology and application*, John Wiley & Sons, Ltd., New Jersey (2012).
35. Q. Song, S. Cao, P. Z. Rivera, L. P. Lu, W. Li, Y. Ji, S. A. Al-Muhtaseb, A. K. Cheetham and E. Sivaniah, *Nat. Commun.*, **4**, 1918 (2013).
36. L. H. Sperling, *Introduction to physical polymer science*, John Wiley & Sons, Ltd., New Jersey (2006).
37. Y. Yampolskii, I. Pinnau and B. Freeman, *Materials science of membranes for gas and vapor separation*, John Wiley & Sons, Ltd., New Jersey (2006).
38. L. M. Robeson, *J. Membr. Sci.*, **320**, 390 (2008).

Supporting Information

Intrinsically microporous oligomers as organic porogens for mixed-matrix membranes

Gi Hyeon Moon, Sungjin Park, Seul Chan Park, Byung Su Kim, Jaeyoung Jang, and Yong Soo Kang†

Department of Energy Engineering, Hanyang University, Seoul 04763, Korea
(*Received 12 December 2019 • accepted 28 February 2020*)

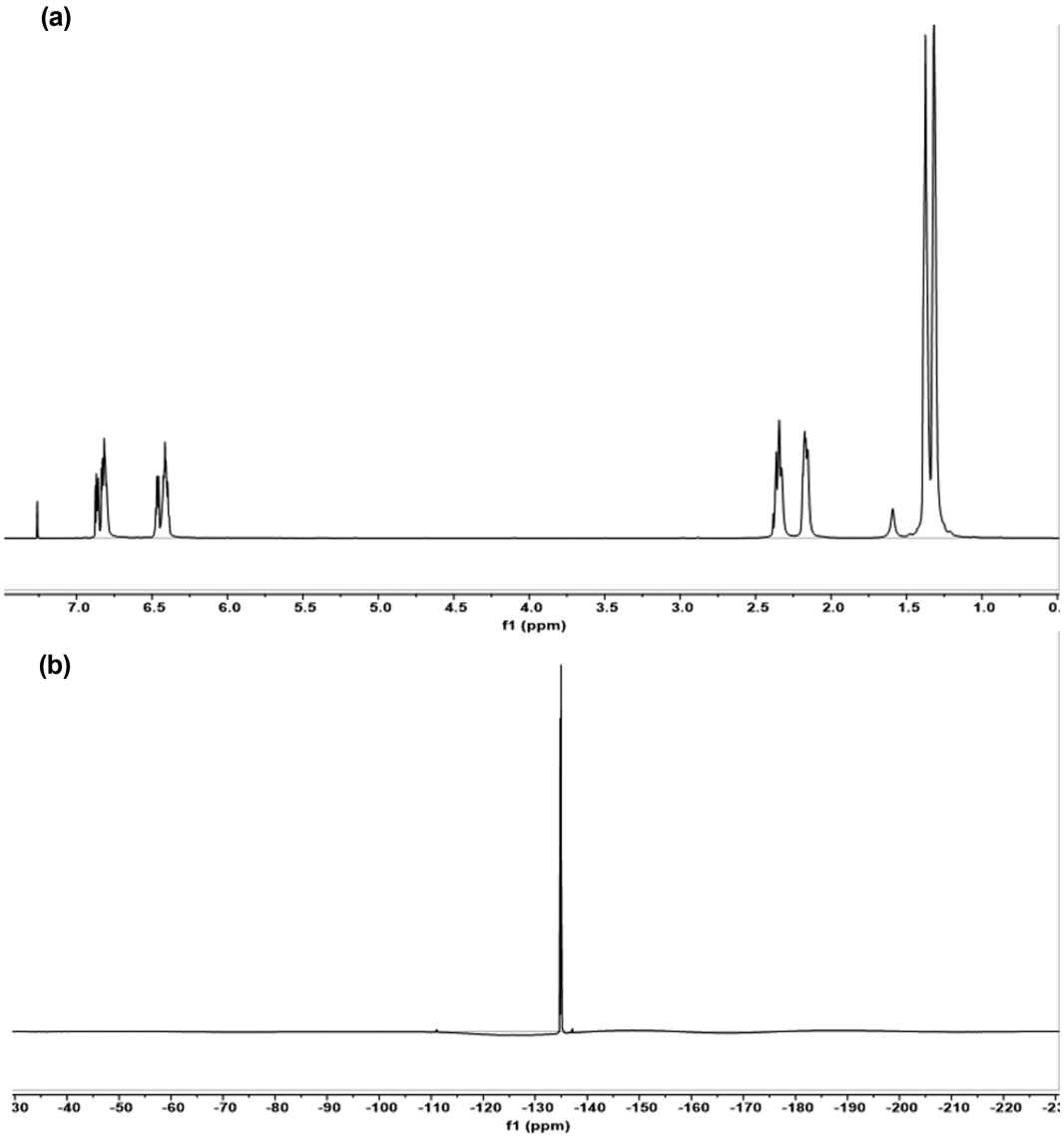


Fig. S1. (a) ^{1}H and (b) ^{19}F NMR spectra of F-OIM.

Gibbs Free Energy of Mixing Of Polymers

Gibbs free energy of mixing of polymers could express as Eq. (3)

$$\Delta G_m = \Delta H_m - T\Delta S_m \quad (3)$$

and entropy of mixing is expressed as Eq. (4)

$$\Delta S_m = -R\left(\frac{v_1}{x_1}\ln v_1 + \frac{v_2}{x_2}\ln v_2\right) \quad (4)$$

Where v_i=volume fraction of component *i*, x=the degree of polymers. The oligomers having smaller x than polymers with larger x

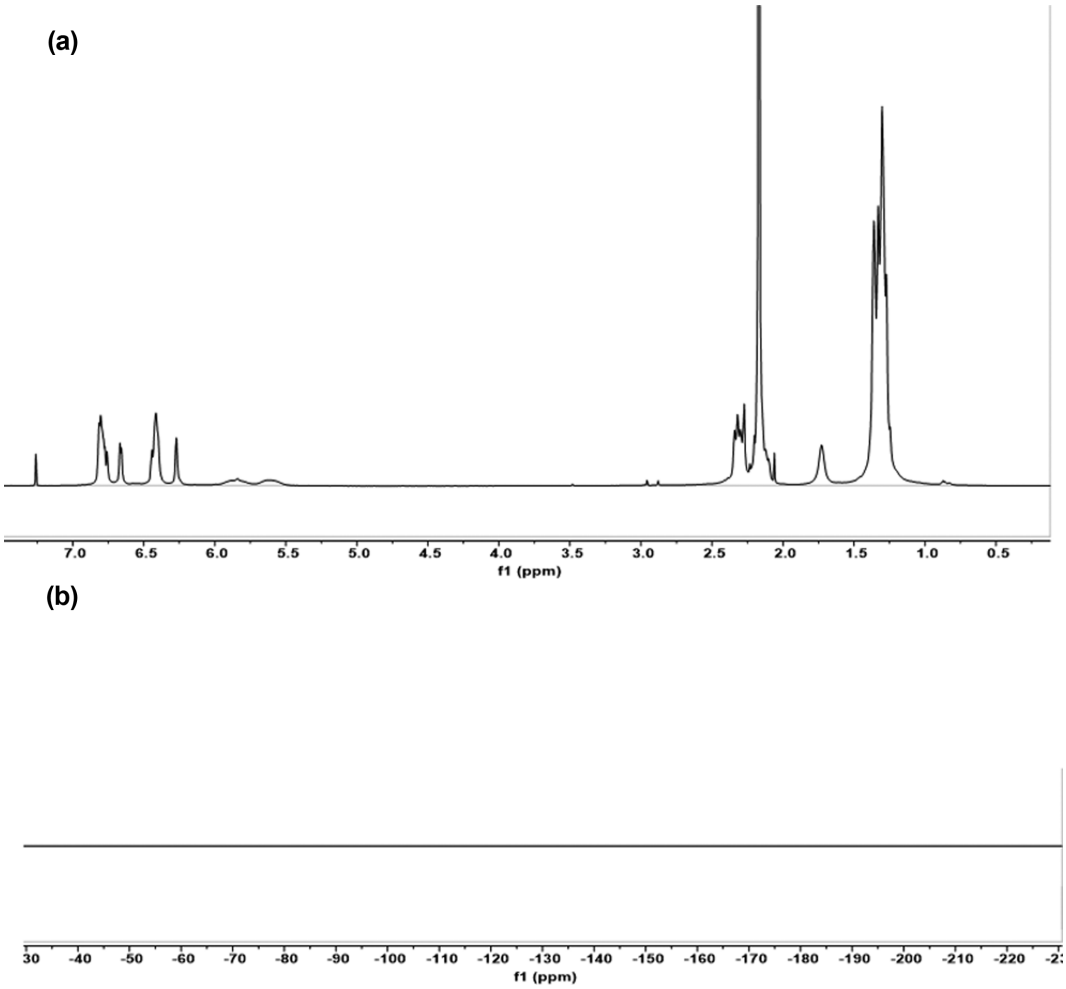


Fig. S2. (a) ^{1}H and (b) ^{19}F NMR spectra of OH-OIM.

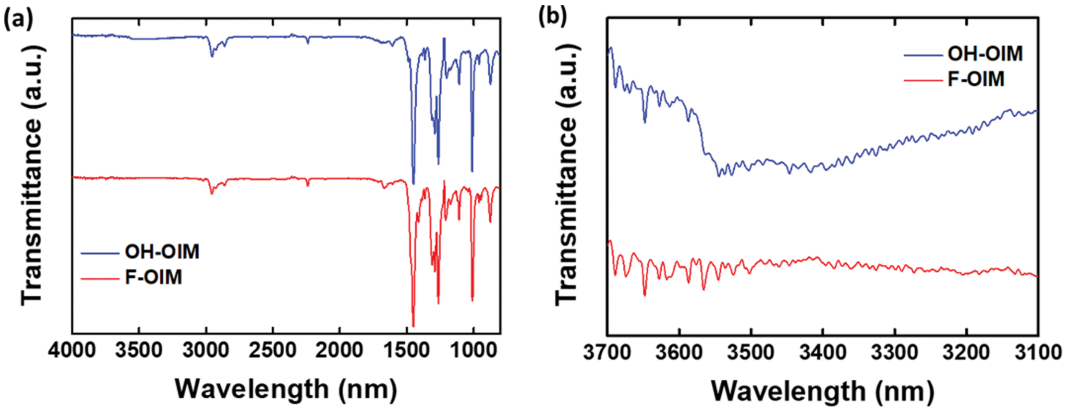


Fig. S3. (a) FT-IR spectra and (b) magnified hydroxyl group regions (3,100-3,700 cm^{-1}) of OH-OIM and F-OIM.

will have large ΔS_m values.

Therefore, the entropy contribution (favorable to compatibility) is getting higher with smaller x.

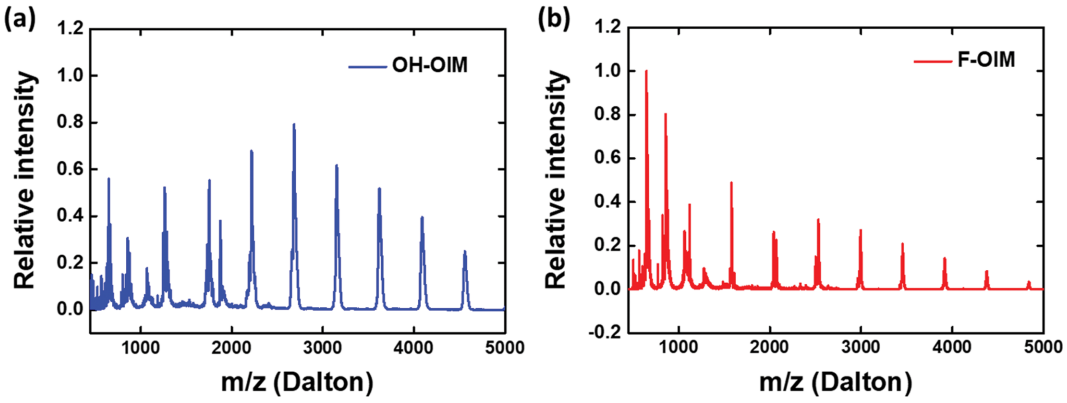


Fig. S4. MALDI-ToF mass spectrum of (a) OH-OIM and (b) F-OIM.

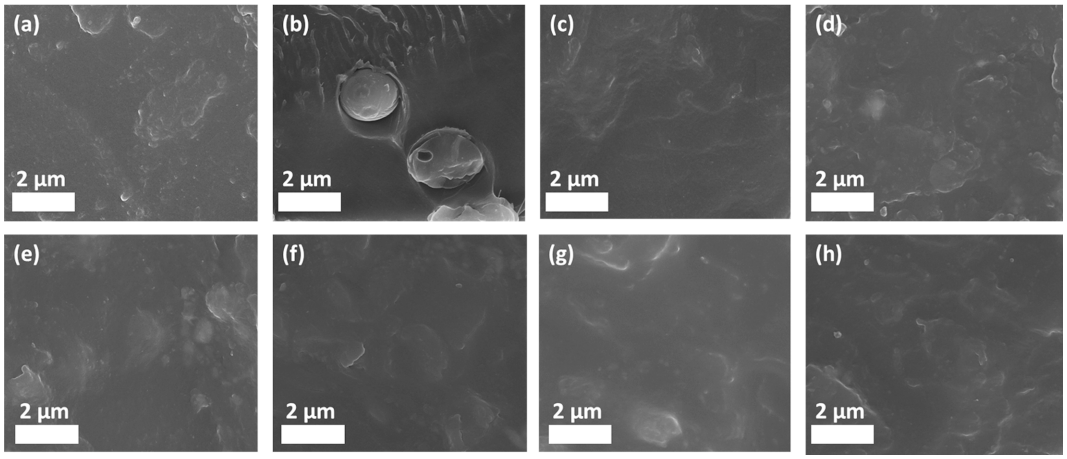


Fig. S5. SEM cross-sectional images of (a) neat PSU, (b) 20 wt% PIM-1/PSU MMMs, OH-OIM/PSU MMMs with (c) 10, (d) 20, (e) 30 wt% of OH-OIM contents, F- OIM/PSU MMMs with (f) 10, (g) 20, (h) 30 wt% of F-OIM contents.

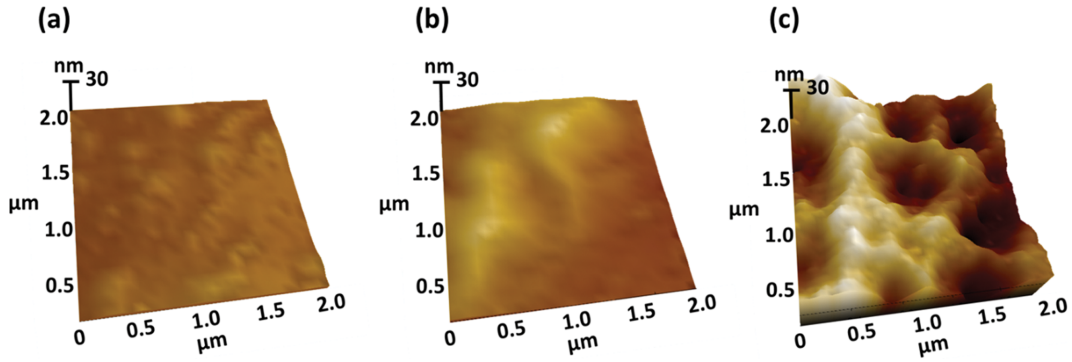


Fig. S6. AFM surface images of (a) OH-OIM/PSU, (b) F-OIM/PSU, and (c) PIM-1/PSU at fixed 20/80 wt% concentrations.

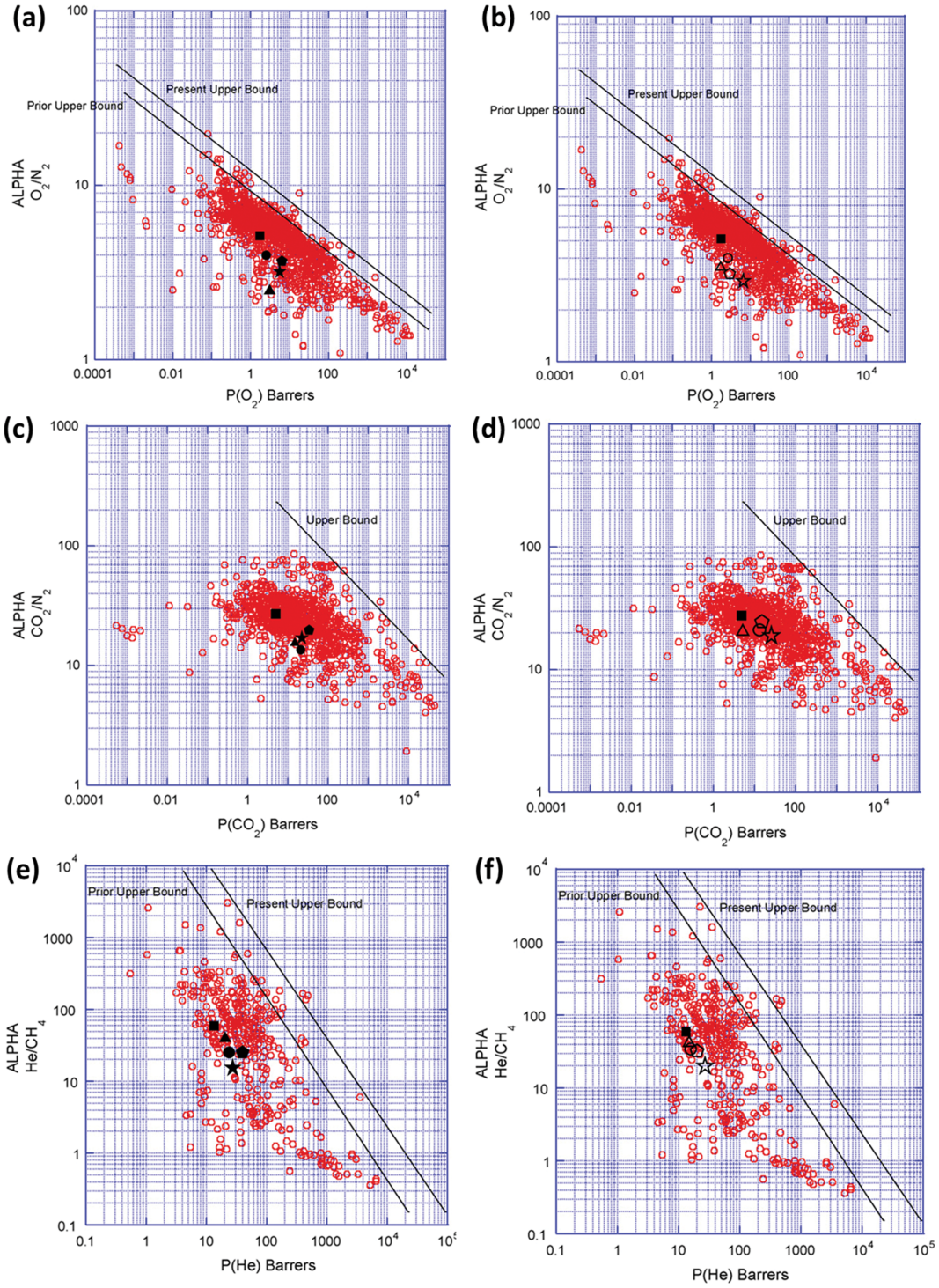


Fig. S7. Plotted gas separation performances of OIM/PSU MMMs on 2008 Robeson upper bound with O_2/N_2 (a), (b), CO_2/N_2 (c), (d), He/CH_4 (e), (f) mixtures. Solid square means neat PSU membranes and solid triangle (10 wt%), circle (15 wt%), pentagon (20 wt%), star (30 wt%) shapes are OH-OIM/PSU MMMs. Hollow shapes mean F-OIM/PSU MMMs with same contents.